An Adaptive Dead-Time Compensation Strategy for Voltage Source Inverter Fed Motor Drives

Naomitsu Urasaki, *Member, IEEE*, Tomonobu Senjyu, *Member, IEEE*, Katsumi Uezato, and Toshihisa Funabashi, *Senior Member, IEEE*

***Abstract*—This paper presents an adaptive dead-time compensation strategy to obtain fundamental phase voltage for inverter fed vector controlled permanent magnet synchronous motor drives. The amplitude of phase dead-time compensation voltage (DTCV) to compensate disturbance voltage due to undesirable characteristics of inverter, such as dead-time, turn-on/off time of switching devices, and on-voltages of switching devices and diodes is adaptively determined according to a dead-time compensation time (DTCT). DTCT is identified on-line with using a δ-axis disturbance voltage in the current reference frame that is synchronized with current vector. The δ-axis disturbance voltage is estimated by a disturbance observer. The accuracy of identified DTCT is experimentally confirmed by calculating the mean absolute percentage error (MAPE) between a calculated active power and a measured one. MAPE for adaptive DTCT is almost within 5% at any operating point.**

***Index Terms*—Current vector, dead-time, disturbance observer, permanent magnet synchronous motor (PMSM), voltage source inverter (VSI).**

I. Introduction

VOLTAGE SOURCE INVERTER (VSI) fed vector controlled motor drives have been widely developed. Several applications, such as rotor position sensorless drives strategy [1], [2] and direct torque control strategy [3] need information on fundamental phase voltage. Since fundamental phase voltage cannot be detected directly from inverter output terminal, commanded voltage is usually used instead of an actual one. However, commanded voltage never agrees with actual fundamental phase voltage due to undesirable characteristics of VSI, such as dead-time, turn-on/off time of switching devices, and on-voltages of switching devices and diodes. Dead-time is vital to avoid short-circuit of inverter legs. Turn-on/off time and on-voltages inevitably exist in actual devices. To cope with this problem, several authors have made attempt to compensate undesirable characteristics of VSI. Generally undesirable characteristics of VSI are compensated by introducing a dead time compensation voltage (DTCV) along with current polarity [4], [5]. The magnitude of DTCV depends on dead-time compensation time (DTCT) that is composed of dead-time, turn-on/off time, and on-voltages. Since it is difficult to measure these parameters exactly and they can vary with operating conditions [6], [7], it is desirable to identify DTCT. For this reason, a startup identification of DTCT was developed [8]. Although the developed method provides good identification result, it cannot perform on-line because this method requires a particular q-axis current command. Thus, this method cannot completely compensate the variation of DTCT. In [9], the magnitude of DTCV is adapted according to the peak value of phase current. However, this method has the disadvantage that it needs to prepare look-up table. In [10], the magnitude of DTCV is adjusted so as to minimize the harmonic components of phase current. Although this method never relay on properties of VSI and motor model, it has trouble with convergence.

To overcome these problems, an adaptive dead-time compensation method using disturbance observer for permanent magnet synchronous motor (PMSM) drive has been proposed [11]. In this method, dq-axes DTCVs in the rotor reference frame are estimated on-line using the disturbance observer which is developed based on mathematical model of PMSM. Then, estimated dq-axes disturbance voltage are added to dq-axes commanded voltages as DTCVs. Although this method performs well, it has a disadvantage that d-axis current must be zero. This restricts application of this method to only PMSM drive. In addition, an adverse effect of estimation delay on dead-time compensation strategy may occur with increase of driving frequency because the fundamental frequency of dq-axes DTCVs is six times that of the driving frequency.

This paper proposes an extended adaptive dead-time compensation method for voltage source inverter fed PMSM drive. In this paper, $\gamma\delta$-axes DTCVs in the current reference frame that is synchronized with current vector are introduced instead of traditional dq-axes DTCVs for adjusting the amplitude of phase DTCV. When δ-axis is aligned with current vector orientation, γ-axis current is always zero regardless of d-axis current. In this situation, a relationship between δ-axis disturbance voltage due to undesirable characteristics of inverter and DTCT is derived. Based on this relationship, DTCT is identified on-line using the δ-axis disturbance voltage estimated by using a disturbance observer. Adaptive DTCT is utilized for adjusting the amplitude of phase DTCV. The proposed method has advantages as follows: 1) It can be applied to other motor drives (e.g., induction motor drive) because the relationship between δ-axis disturbance voltage and DTCT remains unchanged regardless of any d-axis current. 2) It is lightly affected to the estimation delay of disturbance observer because only the amplitude of phase DTCV is adjusted, that is, the polarity of phase DTCV is perfectly agrees with that of phase current. 3) Only the δ-axis dis-

Manuscript received April 2, 2004; revised February 7, 2005. Recommended by Associate Editor M. A. Rahman.

N. Urasaki, T. Senjyu, and K. Uezato are with the Department of Electrical and Electronic Engineering, University of the Ryukyus, Okinawa 903–0213, Japan (e-mail: urasaki@tec.u-ryukyu.ac.jp).

T. Funabashi is with the Power System Engineering Division Meidensha Corporation, Tokyo 103-8515, Japan.

Digital Object Identifier 10.1109/TPEL.2005.854046

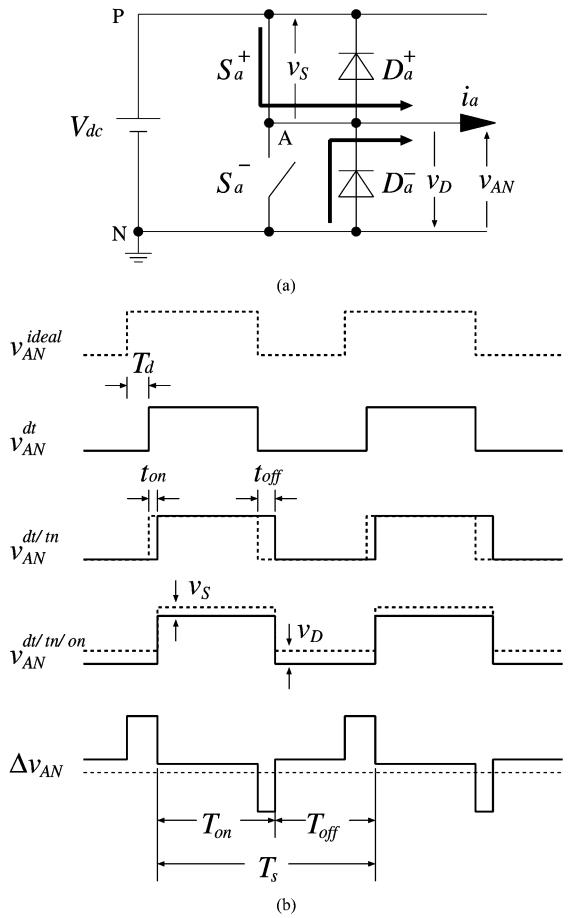

Fig. 1. Relationship between ideal and actual inverter output voltages for $i_a > 0$: (a) Channel flow of a-phase current. (b) Inverter output voltage.

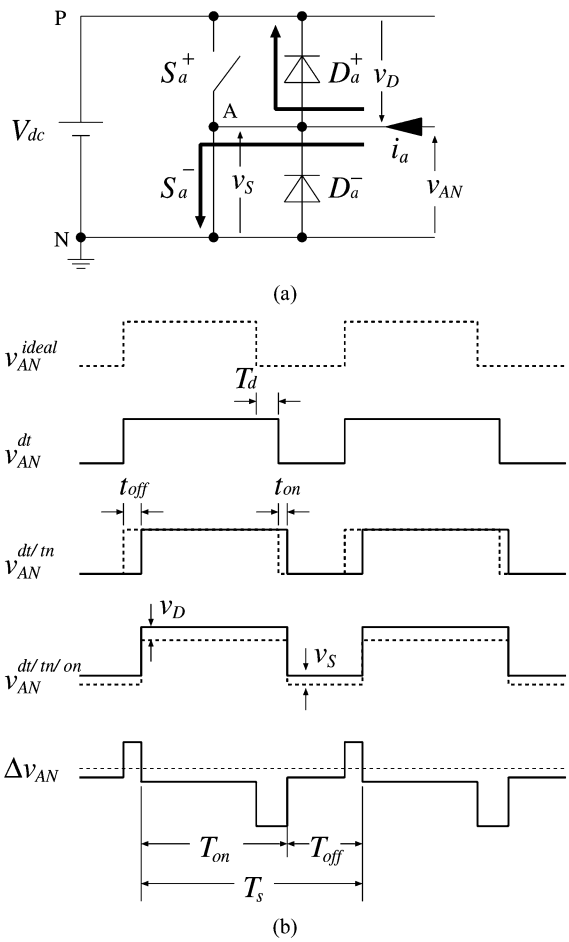

Fig. 2. Relationship between ideal and actual inverter output voltages for $i_a < 0$: (a) Channel flow of a-phase current. (b) Inverter output voltage.

turbance observer is required. Simulation and experimental results are illustrated to confirm the validity and usefulness of the proposed method.

II. Dead-Time Compensation

Fig. 1(a) shows the channel flow of a-phase current for positive direction ($i_a > 0$). The a-phase current i_a flows through switching device S_a^+ during on-period $T_{\rm on}$. On other way, it flows through diode D_a^- during both off-period $T_{\rm off}$ and dead-time T_d, i.e., inverter output voltage $v_{\rm AN}$ for dead-time period is equal to that for off-period. The relationship between ideal and actual inverter output voltages for $i_a > 0$ is shown in Fig. 1(b). Due to dead-time T_d, actual voltage becomes $v_{\rm AN}^{\rm dt}$. In addition, due to turn-on time $t_{\rm on}$ and turn-off time $t_{\rm off}$ of switching device S_a^+, actual voltage becomes $v_{\rm AN}^{\rm dt/tn}$. Furthermore, due to on-voltages v_S of switching device S_a^+ and v_D of diode D_a^-, actual voltage becomes $v_{\rm AN}^{\rm dt/tn/on}$. As a result, the difference between ideal and actual inverter output voltages becomes $\Delta v_{\rm AN}(= v_{\rm AN}^{\rm ideal} - v_{\rm AN}^{\rm dt/tn/on})$.

Fig. 2(a) shows the channel flow of a-phase current for negative direction ($i_a < 0$). The a-phase current i_a flows through switching device S_a^- during off-period $T_{\rm off}$. On other way, it flows through diode D_a^+ during both on-period $T_{\rm on}$ and dead-time T_d, i.e., inverter output voltage $v_{\rm AN}$ for dead-time period is equal to that for on-period. The relationship between ideal and actual inverter output voltages for $i_a < 0$ is shown in Fig. 2(b). From a similar analysis, the difference between ideal and actual inverter output voltages becomes $\Delta v_{\rm AN}(= v_{\rm AN}^{\rm ideal} - v_{\rm AN}^{\rm dt/tn/on})$.

To compensate undesirable characteristics of inverter, a DTCV is added to the commanded voltage generated with current controller in vector controlled PMSM drive system. Since DTCV corresponds to an average value of $\Delta v_{\rm AN}$ over switching period T_s, a-phase DTCV $v_a^{\rm com}$ is derived from the above analytical result as

$$v_a^{\rm com} = \frac{T_c}{T_s} V_{\rm dc}\,{\rm sgn}(i_a) \tag{1}$$

where T_c, T_s, and $V_{\rm dc}$ are DTCT, switching period, and dc-link voltage, respectively. DTCT is defined as

$$T_c = T_d + t_{\rm on} - t_{\rm off} + \frac{V_{\rm on}}{V_{\rm dc}} T_s \tag{2}$$

where $T_d, t_{\rm on}, t_{\rm off}$, and $V_{\rm on}$ are dead-time, turn-on time, turn-off time, and average on-voltage, respectively. The average on-voltage $V_{\rm on}$ is defined as

$$V_{\rm on} = \begin{cases} \frac{T_{\rm on}}{T_s} v_S + \frac{T_{\rm off}}{T_s} v_D & \text{for } i_a > 0 \\ \frac{T_{\rm off}}{T_s} v_S + \frac{T_{\rm on}}{T_s} v_D & \text{for } i_a < 0 \end{cases} \tag{3}$$

where v_D, v_S are on-voltages of diodes and switching devices and $T_{\rm on}, T_{\rm off}$ are on-period and off-period of the upper-arm of inverter leg, respectively. Note that both average on-voltages for positive and negative current directions are almost same because on-period $T_{\rm on}$ for $i_a > 0$ is almost identical to off-period

TABLE I
SPECIFICATIONS OF TESTED INVERTER

maximum rated voltage	V_{CE}	600 V
maximum rated current	I_C	30 A
dead-time for IGBT	T_d	5.0 μs
turn-on time of IGBT	t_{on}	0.6 μs
turn-off time of IGBT	t_{off}	2.0 μs
on-voltage of IGBT	v_S	1.9 V
on-voltage of diode	v_D	2.5 V

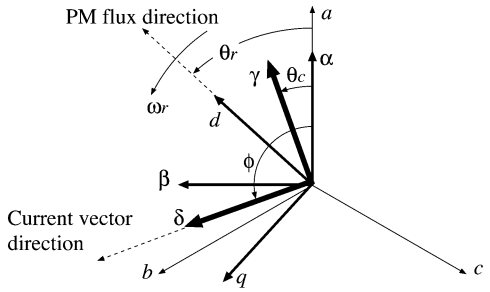

Fig. 3. Definition of coordinate axes.

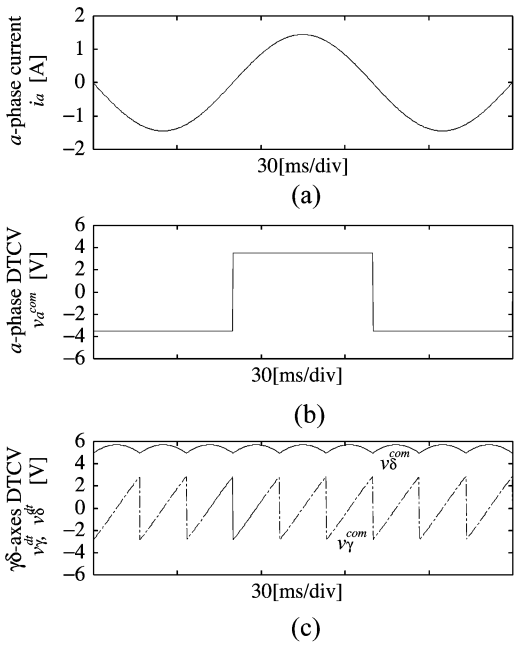

Fig. 4. Relationship between phase DTCV and $\gamma\delta$-axes DTCVs (300 rpm, 1 A, $i_d = -1$ A): (a) a-phase current, (b) a-phase DTCV, and (c) $\gamma\delta$-axes DTCVs.

$T_{\rm off}$ for $i_a < 0$, and vice versa. Similarly, b-phase and c-phase DTCVs are also formulated.

Table I shows the specifications of tested inverter. An insulated gate bipolar transistor (IGBT) module is utilized for switching devices. The dead-time for IGBT is set at 5 μs. In the tested inverter, on-voltage of diode is greater than that of IGBT ($v_D > v_S$). On this condition, as can be seen from (3), average on-voltage $V_{\rm on}$ for $i_a > 0$ decreases with increasing rotor speed because on-period $T_{\rm on}$ increases with inverter output voltage, i.e., $V_{\rm on}$ depends on v_S rather than v_D. A similar explanation is valid for $i_a < 0$. Thus, average on-voltage varies with operating point. In addition, turn-off time $t_{\rm off}$ also varies with operating point due to parasitic capacitors [7]. In other words, DTCT varies with operating point. Since it is difficult to measure parameters listed in Table I individually at various operating points, DTCT formulated in (2) is identified online in this paper.

III. IDENTIFICATION OF DEAD-TIME COMPENSATION TIME

A. Definition of Coordinate Axes

Fig. 3 shows the definition of four coordinate axes. "abc" is defined as flux direction due to each phase current. "$\alpha\beta$" is a stationary reference frame. "dq" is the rotor reference frame that is synchronized with the rotor of PMSM. "$\gamma\delta$" is the current reference frame that is synchronized with current vector. The position angle of $\gamma\delta$-axes is expressed as

$$\theta_c = \phi - \frac{\pi}{2} \tag{4}$$

where ϕ is the position angle of current vector and is expressed as

$$\phi = \tan^{-1}\left(\frac{i_\beta}{i_\alpha}\right) \tag{5}$$

where i_α and i_β are $\alpha\beta$-axes currents.

B. $\gamma\delta$-Axes Dead-Time Compensation Voltages

Fig. 4 shows numerical results of DTCV for inverter fed PMSM drive. In this numerical results, the rotor speed of PMSM is 300 rpm (driving frequency is 10 Hz). The d-axis current i_d is set at -1 A. DTCT T_c, switching period T_s, and dc-link voltage $V_{\rm dc}$ are set at 3.5 μs, 200 μs, and 200 V, respectively. Fig. 4(a) shows a-phase current i_a. The RMS value of phase current is 1 A. Since the polarity of phase DTCV depends on that of phase current, a-phase DTCV $v_a^{\rm com}$ is determined from (1) as shown in Fig. 4(b). Although waveforms of b-phase and c-phase DTCVs are not shown in this figure, they are also determined in a similar way. Phase DTCVs $(v_a^{\rm com}, v_b^{\rm com}, v_c^{\rm com})$ are transformed into $\gamma\delta$-axes DTCVs $(v_\gamma^{\rm com}, v_\delta^{\rm com})$ using the transformation matrix given as

$$\mathbf{C} = \sqrt{\frac{2}{3}}\begin{bmatrix} \cos\theta_c & \cos\left(\theta_c - \frac{2}{3}\pi\right) & \cos\left(\theta_c + \frac{2}{3}\pi\right) \\ -\sin\theta_c & -\sin\left(\theta_c - \frac{2}{3}\pi\right) & -\sin(\theta_c + \frac{2}{3}\pi) \end{bmatrix}. \tag{6}$$

As can be seen from Fig. 4(c), δ-axis DTCV $v_\delta^{\rm com}$ is dc voltage with pulsation. The maximum value of δ-axis DTCV is given as

$$V_{\max}^{\rm com} = 2\sqrt{\frac{2}{3}}\frac{T_c}{T_s}V_{\rm dc}. \tag{7}$$

On the other hand, γ-axis DTCV $v_\gamma^{\rm com}$ is ac voltage. Its amplitude corresponds to $V_{\max}^{\rm com}/2$. The fundamental frequency of $\gamma\delta$-axes DTCVs is six times of driving frequency.

C. Identification of Dead-Time Compensation Time

Manipulating (7) gives the analytical equation of DTCT as

$$T_c = \frac{\sqrt{6}}{4}\frac{V_{\max}^{\rm com}}{V_{\rm dc}}T_s. \tag{8}$$

TABLE II
THEORETICAL $\gamma\delta$-AXES DTCVs

θ_c	v_γ^{com}	v_δ^{com}
$0<\theta_c\leq\frac{\pi}{3}$	$-V_{\max}^{com}\cos(\theta_c+\frac{\pi}{3})$	$V_{\max}^{com}\sin(\theta_c+\frac{\pi}{3})$
$\frac{\pi}{3}<\theta_c\leq\frac{2}{3}\pi$	$-V_{\max}^{com}\cos\theta_c$	$V_{\max}^{com}\sin\theta_c$
$\frac{2}{3}\pi<\theta_c\leq\pi$	$-V_{\max}^{com}\cos(\theta_c-\frac{\pi}{3})$	$V_{\max}^{com}\sin(\theta_c-\frac{\pi}{3})$
$\pi<\theta_c\leq\frac{4}{3}\pi$	$V_{\max}^{com}\cos(\theta_c+\frac{\pi}{3})$	$-V_{\max}^{com}\sin(\theta_c+\frac{\pi}{3})$
$\frac{4}{3}\pi<\theta_c\leq\frac{5}{3}\pi$	$V_{\max}^{com}\cos\theta_c$	$-V_{\max}^{com}\sin\theta_c$
$\frac{5}{3}\pi<\theta_c\leq2\pi$	$V_{\max}^{com}\cos(\theta_c-\frac{\pi}{3})$	$-V_{\max}^{com}\sin(\theta_c-\frac{\pi}{3})$

Since dc-link voltage $V_{\rm dc}$ and switching period T_s are known parameters, maximum δ-axis DTCV $V_{\max}^{\rm com}$ is estimated for the sake of the calculation of DTCT. It is assumed that undesirable characteristics of inverter yield $\gamma\delta$-axes disturbance voltages $(v_\gamma^{\rm dt}, v_\delta^{\rm dt})$ in current control loop of vector controlled PMSM drive system. A disturbance observer estimates δ-axis disturbance voltage. Since δ-axis disturbance voltage $v_\delta^{\rm dt}$ to be compensated corresponds to δ-axis DTCV $v_\delta^{\rm com}$, the maximum value of the estimated δ-axis disturbance voltage is regarded as $V_{\max}^{\rm com}$. However, it is difficult to estimate reliable maximum value of δ-axis disturbance voltage when estimated δ-axis disturbance voltage chatters. In order to overcome this problem, average δ-axis DTCV $V_{\rm ave}^{\rm com}$ is utilized for identifying DTCT. Table II summarizes the theoretical $\gamma\delta$-axes DTCVs for angle θ_c. From Table II, δ-axis DTCV averaged over $\pi/3$ rad is derived as

$$V_{\rm ave}^{\rm com}=\frac{3}{\pi}V_{\max}^{\rm com}\int_0^{\pi/3}\sin\left(\theta_c+\frac{\pi}{3}\right)d\theta_c=\frac{3}{\pi}V_{\max}^{\rm com}. \quad (9)$$

From (8) and (9), the relationship between DTCT T_c and average δ-axis DTCV $V_{\rm ave}^{\rm com}$ is derived as

$$T_c=\frac{\pi}{3}\frac{\sqrt{6}}{4}\frac{V_{\rm ave}^{\rm com}}{V_{\rm dc}}T_s. \quad (10)$$

As can be seen from Table II, $V_{\max}^{\rm com}$ can be estimated using γ-axis disturbance voltage because it is also related to γ-axis DTCV $v_\gamma^{\rm com}$. However, as compared with estimating δ-axis DTCV, a larger pole of observer is required to estimate γ-axis DTCV because γ-axis DTCV is ac voltage. A system stability point of view, a large pole must be avoided. In addition, since the average value of γ-axis DTCV is theoretically equal to zero, it has no use for identification of DTCT. For above reasons, δ-axis disturbance voltage is utilized for identifying DTCT.

D. Estimation of δ-Axis Disturbance Voltage

This paper focuses on dead-time compensation for vector controlled PMSM drive. Disturbance observer for estimating δ-axis disturbance voltage is developed from the voltage equation of PMSM in $\gamma\delta$-axes. The voltage equation is given as

$$\left.\begin{aligned}v_\gamma&=Ri_\gamma+Lpi_\gamma+v_{\gamma d}\\ v_\delta&=Ri_\delta+Lpi_\delta+v_{\delta d}\end{aligned}\right\} \quad (11)$$

where $v_\gamma, v_\delta, i_\gamma, i_\delta, R, L$, and p are $\gamma\delta$-axes voltages and currents, armature resistance, armature inductance, and differential operator, respectively. Decoupling voltages are defined as

$$\left.\begin{aligned}v_{\gamma d}&=-\omega_r\{Li_\delta+K_e\sin(\theta_c-\theta_r)\}\\ v_{\delta d}&=\omega_r\{Li_\gamma+K_e\cos(\theta_c-\theta_r)\}\end{aligned}\right\} \quad (12)$$

where ω_r, θ_r, and K_e are electrical angular velocity, the position angle of rotor, and emf constant, respectively.

The commanded voltage generated with current controller without dead-time compensation strategy increases by disturbance voltages $(v_\gamma^{\rm dt}, v_\delta^{\rm dt})$ to reduce current error against the disturbance voltage. The voltage equation for current control loop is expressed as

$$\left.\begin{aligned}v_\gamma^*&=Ri_\gamma+Lpi_\gamma+v_{\gamma d}+v_\gamma^{\rm dt}\\ v_\delta^*&=Ri_\delta+Lpi_\delta+v_{\delta d}+v_\delta^{\rm dt}\end{aligned}\right\} \quad (13)$$

where superscript "$*$" denotes commanded value. As a result, the commanded voltage disagrees with actual one, i.e., (13) disagrees with (11).

By contrast, the commanded voltages with dead-time compensation strategy are expressed as

$$\left.\begin{aligned}v_\gamma^*+v_\gamma^{\rm com}&=Ri_\gamma+Lpi_\gamma+v_{\gamma d}+v_\gamma^{\rm dt}\\ v_\delta^*+v_\delta^{\rm com}&=Ri_\delta+Lpi_\delta+v_{\delta d}+v_\delta^{\rm dt}\end{aligned}\right\}. \quad (14)$$

As can be seen from (14), the commanded voltage (v_δ^*, v_γ^*) corresponds to actual one provided that $\gamma\delta$-axes DTCVs $(v_\gamma^{\rm com}, v_\delta^{\rm com})$ agree with $\gamma\delta$-axes disturbance voltages $(v_\gamma^{\rm dt}, v_\delta^{\rm dt})$.

In the proposed method, δ-axis disturbance observer is developed because only δ-axis disturbance voltage is utilized for identifying DTCT. Assuming that δ-axis disturbance voltage seldom changes during control period, i.e., $\dot{v}_\delta^{\rm dt}=0$, the state and output equations of PMSM taking disturbance voltage into account are expressed as

$$\dot{\boldsymbol{x}}=\frac{d}{{\rm dt}}\begin{bmatrix}i_\delta\\ v_\delta^{\rm dt}\end{bmatrix}=\begin{bmatrix}-\frac{R}{L} & -\frac{1}{L}\\ 0 & 0\end{bmatrix}\begin{bmatrix}i_\delta\\ v_\delta^{\rm dt}\end{bmatrix}+\begin{bmatrix}\frac{1}{L}\\ 0\end{bmatrix}(v'_\delta-v_{\delta d}) \quad (15)$$

$$\boldsymbol{y}=[1\quad 0]\begin{bmatrix}i_\delta\\ v_\delta^{\rm dt}\end{bmatrix} \quad (16)$$

where $v'_\delta=v_\delta^*+v_\delta^{\rm com}$, $\boldsymbol{x}$ and $\boldsymbol{y}$ are state vector and output vector, respectively.

From (15) and (16), disturbance observer is developed as

$$\begin{aligned}\dot{\hat{\boldsymbol{x}}}&=\frac{d}{{\rm dt}}\begin{bmatrix}\hat{i}_\delta\\ \hat{v}_\delta^{\rm dt}\end{bmatrix}\\ &=\begin{bmatrix}-G_1-\frac{R}{L} & -\frac{1}{L}\\ -G_2 & 0\end{bmatrix}\begin{bmatrix}\hat{i}_\delta\\ \hat{v}_\delta^{\rm dt}\end{bmatrix}+\begin{bmatrix}G_1\\ G_2\end{bmatrix}i_\delta\\ &\quad+\begin{bmatrix}\frac{1}{L}\\ 0\end{bmatrix}(v'_\delta-v_{\delta d})\end{aligned} \quad (17)$$

where $G_1=-(R/L+\gamma_1+\gamma_2), G_2=-L\gamma_1\gamma_2, \gamma_1$, and γ_2 are poles of observer.

IV. SYSTEM CONFIGURATION

Fig. 5 shows vector controlled PMSM drive system. The proposed dead-time compensator is indicated by dashed block. The flow chart of the proposed dead-time compensation is shown in Fig. 6:

Step 1) The δ-axis voltage v'_δ and δ-axis current i_δ are obtained from corrected commanded voltages (v'_a, v'_b, v'_c) and phase currents (i_a, i_b, i_c) by coordinate transformation.

Step 2) The δ-axis disturbance voltage $v_\delta^{\rm dt}$ is estimated by the disturbance observer indicated in (17).

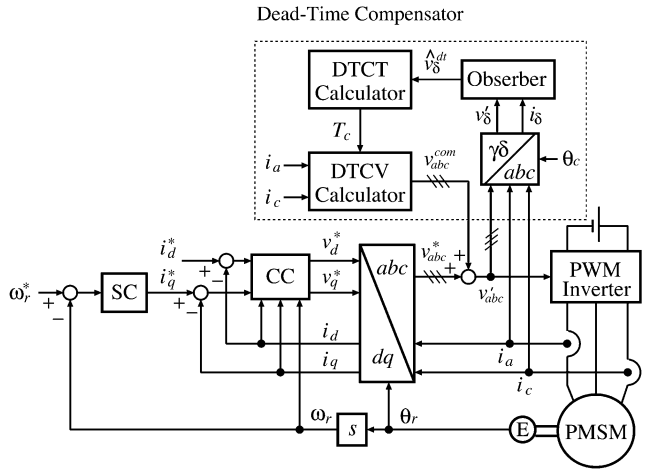

Fig. 5. Vector controlled PMSM drive system for variable speed drive with adaptive dead-time compensation strategy.

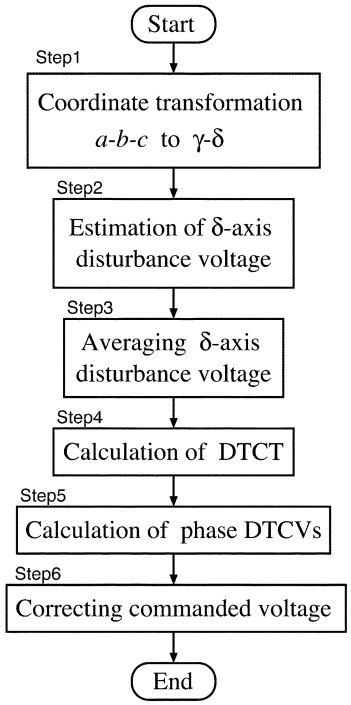

Fig. 6. Flow chart of the proposed dead-time compensator.

Step 3) Estimated δ-axis disturbance voltage is averaged by the procedure illustrated in Fig. 7.

1) Estimated δ-axis disturbance voltage $\hat{v}_\delta^{\mathrm{dt}}$ is integrated during the interval from t_k to t_{k+n_1}. Here, sampling points t_k and t_{k+n_1} mean the first and second zero cross points of a-phase current i_a, respectively.
2) At sampling point t_{k+n_1}, integrated δ-axis disturbance voltage is averaged as

$$V_{\mathrm{ave}}^{\mathrm{com}} = \frac{\sum \hat{v}_\delta^{\mathrm{dt}}}{n_1} \tag{18}$$

3) $V_{\mathrm{ave}}^{\mathrm{com}}$ is utilized for identification of DTCT during the interval from t_{k+n_1} to t_{k+n_2}.
4) $V_{\mathrm{ave}}^{\mathrm{com}}$ is updated at sampling point t_{k+n_2} and utilized during the interval from t_{k+n_2} to t_{k+n_3}, sequentially.

Step 4) DTCT T_c is calculated from (10) using the averaged disturbance voltage $V_{\mathrm{ave}}^{\mathrm{com}}$.

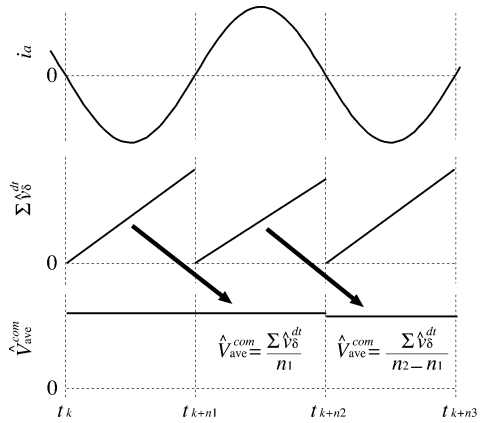

Fig. 7. Average method for δ-axis disturbance voltage.

TABLE III
SPECIFICATIONS OF TESTED PMSM

rated power	P_n	160 W
rated torque	τ_n	0.5 N·m
maximum rated speed	N_n	3,000 rpm
armature resistance	R	2.20 Ω
armature inductance	L	0.0065 H
emf constant	K_e	0.0658 V·s/rad
number of pole-pairs	P	2

TABLE IV
CONTROL PARAMETERS

dc-link voltage	V_{dc}	200 V
carrier frequency	f_c	5 kHz
switching period	T_s	200 μs
control period	T_{ctl}	200 μs
proportional gain for SC	K_{ps}	0.01
integral gain for SC	K_{is}	0.30
proportional gain for CC	K_{pc}	10
integral gain for CC	K_{ic}	1,000
poles of observer	γ_1, γ_2	−2,000

Step 5) The a-phase DTCV v_a^{com} is calculated from (1) using the identified DTCT T_c. Similarly, b-phase and c-phase DTCVs $(v_b^{\mathrm{com}}, v_c^{\mathrm{com}})$ are also calculated.

Step 6) Phase DTCVs $(v_a^{\mathrm{com}}, v_b^{\mathrm{com}}, v_c^{\mathrm{com}})$ are added to commanded voltages (v_a^*, v_b^*, v_c^*). Then, corrected commanded voltage (v_a', v_b', v_c') are utilized for the gate signal of VSI.

V. SIMULATION RESULTS

Table III shows the specifications of tested PMSM employed in this simulation. Two PI controllers are utilized for speed controller (SC) and current controller (CC) in the vector controlled PMSM drive system indicated in Fig. 5. Control parameters are shown in Table IV.

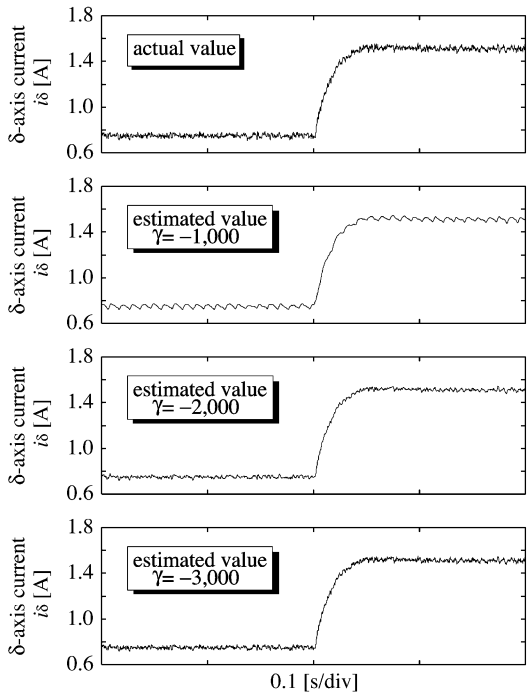

Fig. 8. Simulation results of estimation of δ-axis current for various poles of observer.

The pole of observer has been selected carefully because it affects performance of disturbance observer. In this case, the actual value of δ-axis disturbance voltage cannot be obtained, while the actual value of δ-axis current can be obtained. For this reason, the pole of disturbance observer has been selected based on the accuracy of estimation for δ-axis current. Fig. 8 shows the estimation results of δ-axis current for various poles $\gamma = \gamma_1 = \gamma_2$. For $\gamma = -1,000$, estimation is poor, that is, estimated current pulsates. For $\gamma = -2,000$, δ-axis current is estimated without serious delay. For $\gamma = -3,000$, δ-axis current is estimated well, that is, high frequency components are also estimated. However, high frequency components are not required in the proposed method because estimated δ-axis disturbance voltage is averaged. For system stability point of view, the pole of observer has been conservatively selected at $-2,000$.

Fig. 9 shows simulation result for adjusting the amplitude of phase DTCV. The rotor speed of PMSM is 300 rpm (driving frequency is 10 Hz). In this simulation, d-axis current i_d and DTCT T_c are set at -1A and 3.5 μs, respectively. Fig. 9(a) shows the δ-axis disturbance voltage v_δ^{dt} estimated by disturbance observer. Although estimated δ-axis disturbance voltage (solid line) practically agrees with ideal δ-axis DTCV (dashed line), the maximum value of estimated δ-axis disturbance voltage is greater than that of ideal δ-axis DTCV in some instants. An extreme maximum value results in identification error of DTCT. To overcome this problem, the average value of estimated δ-axis disturbance voltage is utilized for identifying DTCT. As can be confirmed from Fig. 9(b), there is no prominent error between average values of δ-axis disturbance voltage and ideal δ-axis DTCV. Fig. 9(c) shows a-phase DTCV v_a^{com}. The amplitude of the DTCV almost agrees with that of ideal DTCV.

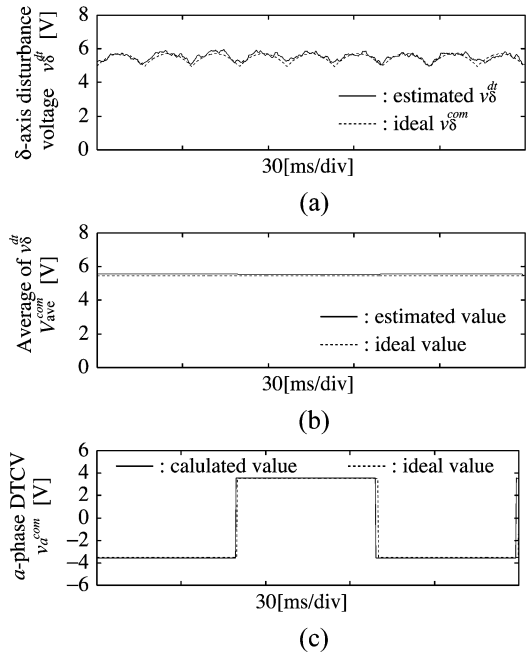

Fig. 9. Simulation results for adjusting the amplitude of phase DTCV (300 rpm, 1 A, $i_d = -1$ A): (a) δ-axis disturbance voltage, (b) average value of δ-axis disturbance voltage, and (c) a-phase DTCV.

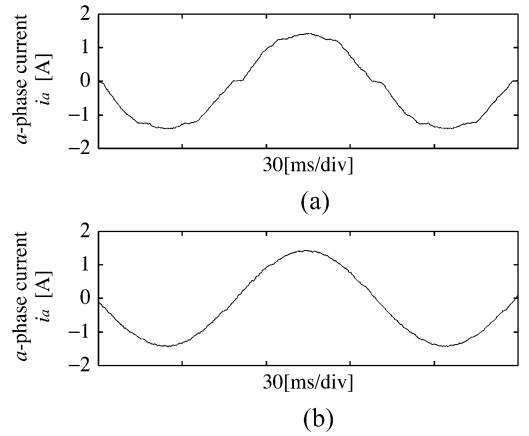

Fig. 10. Simulation results for comparison of a-phase current between (a) without and (b) with the proposed dead-time compensation strategy (300 rpm, 1 A, $i_d = -1$ A).

Fig. 10 shows a-phase current i_a with/without the dead time compensation strategy. As can be seen from Fig. 10(a), a-phase current is distorted due to dead-time effect. Although a high gain current controller suppresses the current distortion, it may deteriorate the stability of the current control system. Furthermore, only a use of high gain current controller cannot clean up discrepancy between actual and commanded voltage even if current distortion is suppressed. On the other hand, as can be confirmed from Fig. 10(b), the distortion of a-phase current is suppressed by applying the proposed dead-time compensation strategy. Note that since the proposed dead-time compensator is a form of feedfoward controller, it provides a stable current control system in comparison with only the feedback current controller.

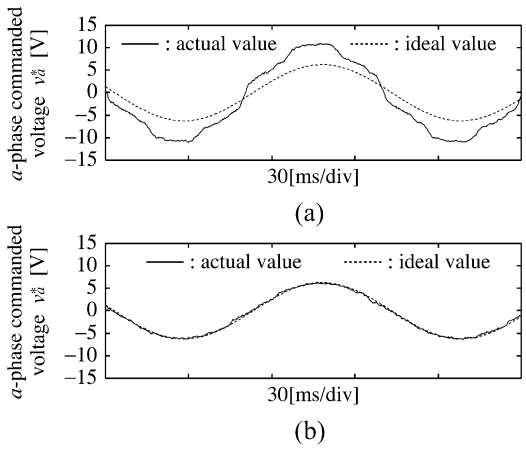

Fig. 11. Simulation results for comparison of a-phase commanded voltage between (a) without and (b) with the proposed dead-time compensation strategy (300 rpm, 1 A, $i_d = -1$ A).

Fig. 11 shows a-phase commanded voltage v_a^* with/without the proposed dead-time compensation strategy. In order to confirm that commanded voltage quantitatively agrees with ideal phase voltage, it is compared with phase voltage when we use an ideal power source (sinusoidal voltage source). Commanded voltage without dead-time compensation strategy disagrees with ideal phase voltage because the commanded voltage is adjusted so as to reduce current error against disturbance voltage due to undesirable characteristics of inverter in feedback current control loop. As a result, the waveform of commanded voltage v_a^* is not sinusoidal any longer. In contrast, the commanded voltage with the proposed dead-time compensation strategy almost agrees with ideal phase voltage. In other words, current controller does not react against disturbance voltage because the proposed dead-time compensator performs well. As a result, the waveform of commanded voltage v_a^* is almost sinusoidal.

VI. Experimental Results

In order to confirm validity of the proposed method, several experiments for the proposed dead-time compensation strategy have been executed. Most of the parts of the system shown in Fig. 5 are implemented in a DSP TMS320C32. The control parameters are same as the simulation.

A. Experimental Results at Medium Speed Condition

Fig. 12 shows experimental results for adjusting the amplitude of phase DTCV. Fig. 12(a) shows estimation result of δ-axis disturbance voltage. It is confirmed from this figure that estimated δ-axis disturbance voltage is dc voltage with pulsation. The fundamental frequency of this pulsation is six times of driving frequency. The estimated δ-axis disturbance voltage is averaged as shown in Fig. 12(b). DTCT is calculated from (10) using the average value of estimated δ-axis disturbance voltage. Then, a-phase DTCV is calculated from (1) as shown in Fig. 12(c).

Fig. 13 shows a-phase current detected through a 12-b AD converter. As can be confirmed from this figure, low-order harmonics of a-phase current are suppressed by applying the

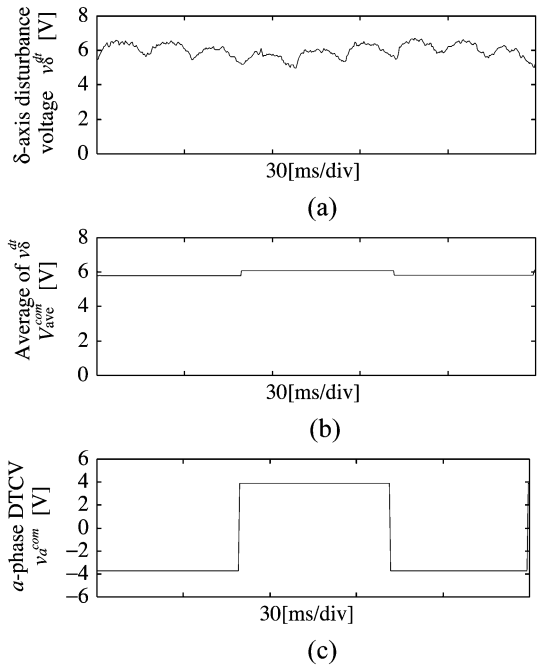

Fig. 12. Experimental results for adjusting the amplitude of phase DTCV (300 rpm, 1 A, $i_d = -1$ A): (a) δ-axis disturbance voltage, (b) average value of δ-axis disturbance voltage, (c) a-phase DTCV.

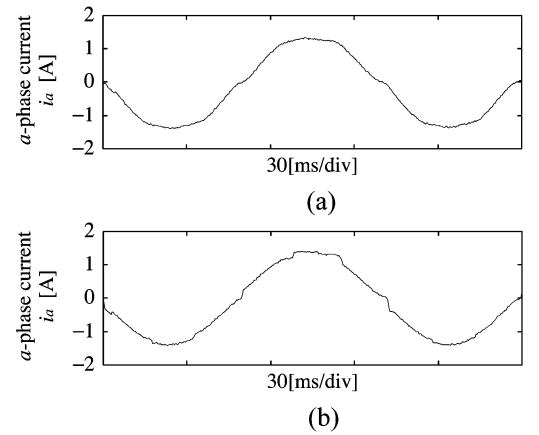

Fig. 13. Experimental results for comparison of a-phase current between (a) without and (b) with the proposed dead-time compensation strategy (300 rpm, 1 A, $i_d = -1$ A).

proposed dead-time compensation strategy. The a-phase commanded voltage v_a^* with the proposed dead-time compensation strategy is compared with the commanded voltage without dead-time compensation strategy in Fig. 14. As can be seen from this figure, disturbance voltage due to undesirable characteristics of inverter is almost removed by applying the proposed dead-time compensation strategy. However, the commanded voltage waveform with the proposed dead-time compensation strategy is slightly distorted every $\pi/3$ rad because zero clamp phenomena of phase current are not perfectly removed even though the dead-time compensation strategy is executed.

Fig. 15 shows identification results of DTCT at various operating points. As expected earlier, identified DTCT tends to decrease with increasing rotor speed. In addition, DTCT also tends to decrease with increasing d-axis current i_d. This can be

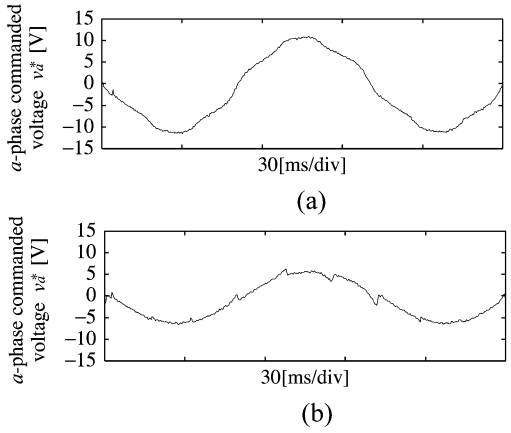

Fig. 14. Experimental results for comparison of a-phase commanded voltage between (a) without and (b) with the proposed dead-time compensation strategy (300 rpm, 1 A, $i_d = -1$ A).

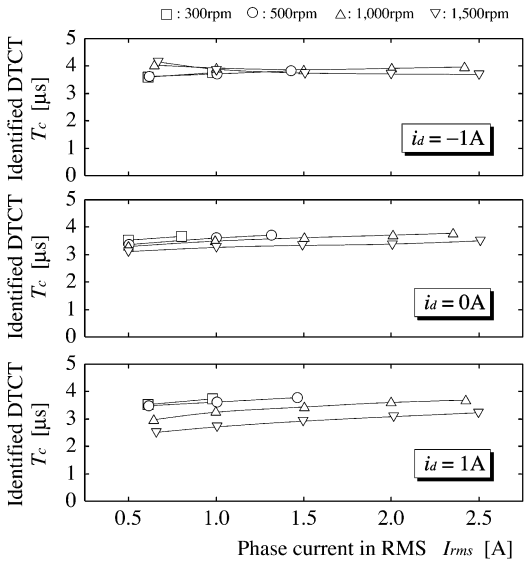

Fig. 15. Experimental results for identifying DTCT at various operating points.

explained as follows: The direction of flux due to positive d-axis current is same as that of flux due to permanent magnet on the rotor of PMSM. In this situation, phase voltage increases, i.e., on-period increases. As discussed in Section II, DTCT for tested inverter decreases with increasing on-period $T_{\rm on}$. Note that the proposed method can be applied to any three phase motor, such as induction motor, so experimental results for positive d-axis current has also been executed even though PMSM usually does not operate at this operating condition. On the other hand, DTCT tends to increase with RMS value of phase current. This can be explained that on-voltages v_D and v_S increase with RMS value of phase current. Note that although on-voltages v_S and v_D are treated as fixed values in this paper, variations of them are implicitly incorporated into the identified DTCT.

In order to evaluate the proposed dead-time compensation strategy quantitatively, active power calculated with using commanded voltage is compared with active power measured with

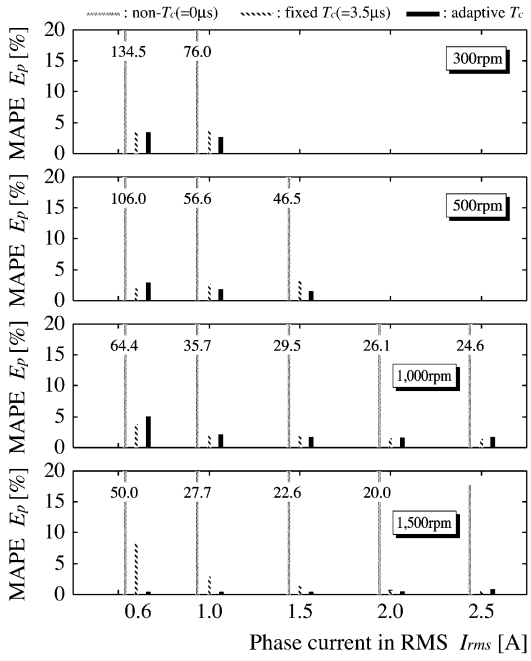

Fig. 16. Comparison between MAPE of calculated and measured active power at various operating points for $i_d = -1$ A.

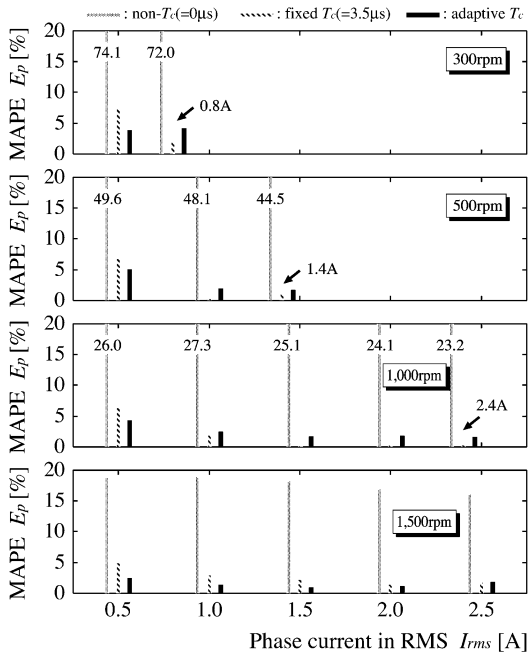

Fig. 17. Comparison between MAPE of calculated and measured active power at various operating points for $i_d = 0$ A.

the help of digital power meter WT230. The calculated active power is obtained from

$$P_{\rm in}^{c} = v_d^* i_d + v_q^* i_q \tag{19}$$

where v_d^*, v_q^*, i_d, and i_q are dq-axes commanded voltages and currents, respectively. Figs. 16–18 show the mean absolute per-

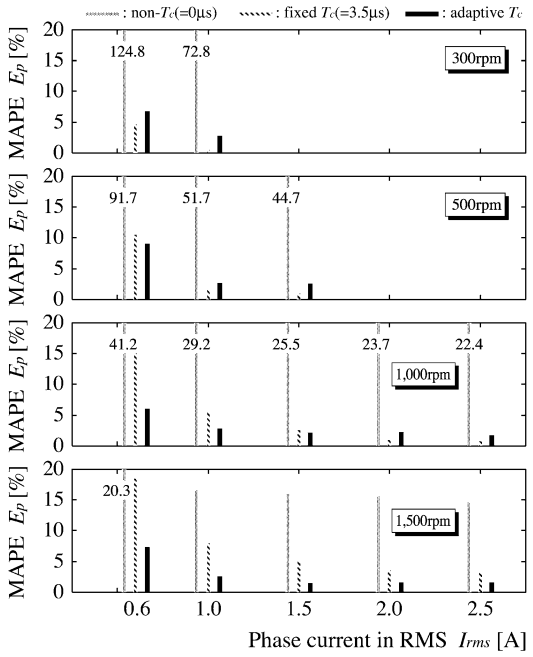

Fig. 18. Comparison between MAPE of calculated and measured active power at various operating points for $i_d = 1$ A.

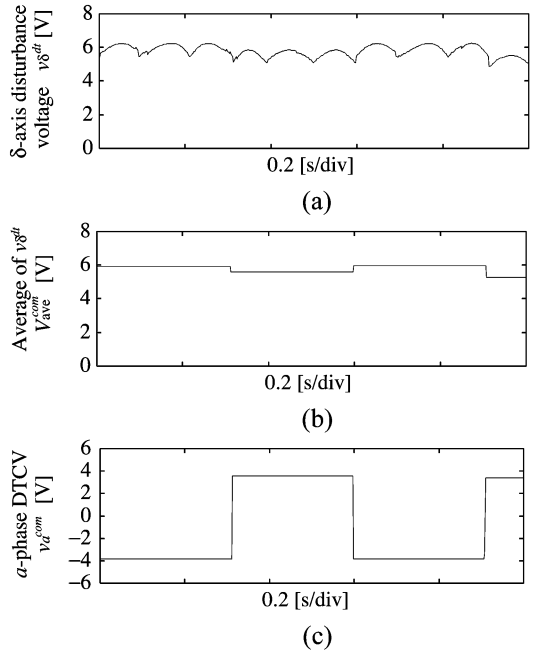

Fig. 19. Experimental results for adjusting the amplitude of phase DTCV (50 rpm, 0.6 A, $i_d = -1$ A). (a) δ-axis disturbance voltage. (b) Average value of δ-axis disturbance voltage. (c) a-phase DTCV.

centage error (MAPE) of calculated active power for various DTCT conditions. MAPE is defined as

$$E_p = \frac{1}{N}\sum_{n=1}^{N}\left(\frac{|P_{\rm in}^c - P_{\rm in}^m|}{P_{\rm in}^m}\right) \times 100 \qquad (20)$$

where $P_{\rm in}^c, P_{\rm in}^m$, and N denote calculated active power, measured active power, and numbers of data, respectively.

Fig. 16 shows MAPE for $i_d = -1$ A. To confirm validity of the proposed method, MAPE for adaptive DTCT is compared with both non-DTCT ($T_c = 0$ μs) and fixed DTCT ($T_c = 3.5$ μs). MAPE for non-DTCT is the largest for any operating point. Note that the value of MAPE for non-DTCT is inscribed in this figure because it exceeds the scale of vertical axis. MAPE for adaptive DTCT is within 5% at any operating point. The fact that MAPE at operating point (1500 rpm, 0.6 A) in which identified DTCT deviate from 3.5 μs is reduced by using adaptive DTCT confirms the validity of identified DTCT.

Fig. 17 shows MAPE for $i_d = 0$ A. Since MAPE for adaptive DTCT in this condition is also within 5%, identified DTCT is valid. Note that MAPE for both adaptive DTCT and fixed DTCT ($T_c = 3.5$ μs) are almost same because identified DTCT in this condition is close to 3.5 μs at any operating point.

Fig. 18 shows the MAPE for $i_d = 1$ A. As can be seen from Fig. 15, identified DTCT decreases with increasing the rotor speed. Since MAPE at 1000 rpm and 1500 rpm is reduced by using adaptive DTCT especially in low current level, the proposed method is valid.

B. Experimental Results at Low Speed Condition

Fig. 19 shows experimental result for adjusting the amplitude of phase DTCV. The disturbance observer performs well under low speed operation: 50 rpm (driving frequency is 1.67 Hz). It can be confirmed from comparison Fig. 20(a) and (b) that low-order harmonics of a-phase current are suppressed by applying the proposed method.

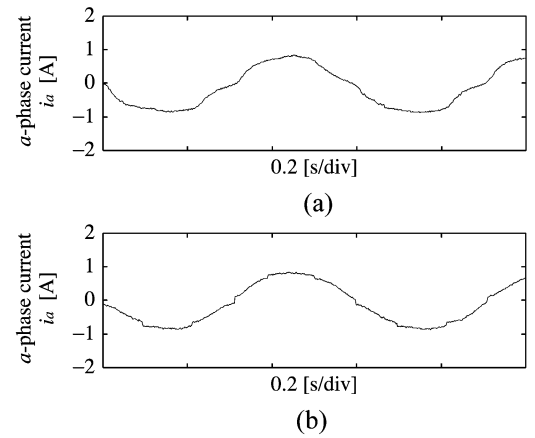

Fig. 20. Experimental results for comparison of a-phase current between (a) without and (b) with the proposed dead-time compensation strategy (50 rpm, 0.6 A, $i_d = -1$ A).

Fig. 21 compares a-phase commanded voltage with/without dead-time compensation. Since commanded voltage in low speed region becomes low, the difference between both waveforms becomes increasingly prominent.

C. Experimental Results in Dynamical Condition

Fig. 22 shows experimental result for the proposed dead-time compensation strategy under dynamical condition. In this case, rotor speed accelerates from 300 rpm to 1,500 rpm. In order to clarify the adaptive performance of the proposed method, the $i_d = 1$ A condition in which DTCT T_c widely varies with operating condition (see Fig. 15) is selected in this experiment.

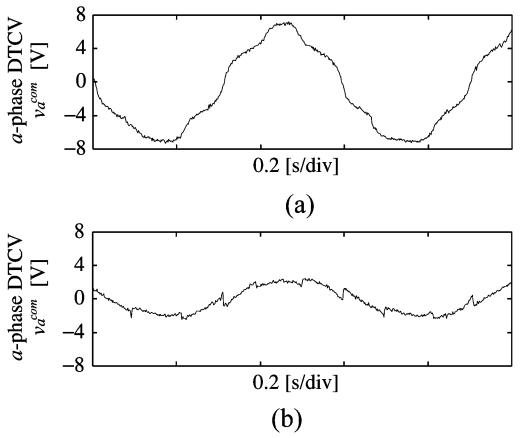

Fig. 21. Experimental results for comparison of a-phase commanded voltage between (a) without and (b) with the proposed dead-time compensation strategy (50 rpm, 0.6 A, $i_d = -1$ A).

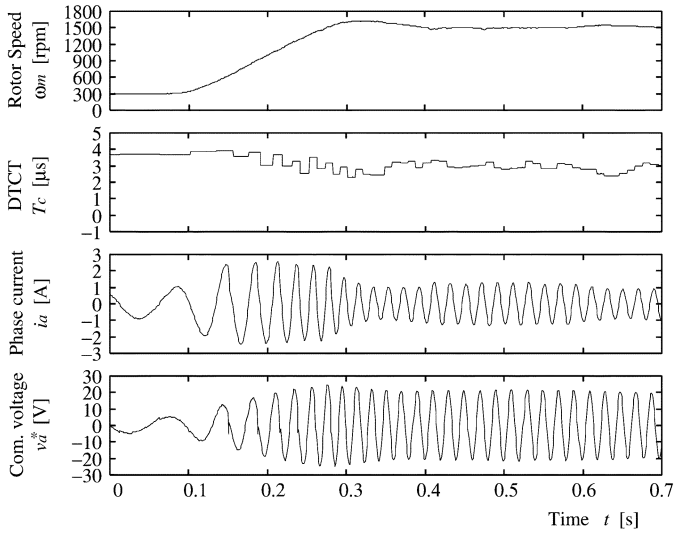

Fig. 22. Experimental results for the proposed dead-time compensation strategy under dynamical condition ($i_d = 1$ A).

As expected from Fig. 15, DTCT T_c quickly decreases with increasing rotor speed, equivalently increasing the amplitude of phase voltage.

VII. Conclusion

This paper has proposed an adaptive dead-time compensation strategy for voltage source inverter fed motor drives. Permanent magnet synchronous motor (PMSM) drive has specifically been discussed in this paper. In the first phase, it was pointed out that dead-time compensation time (DTCT) which includes dead-time, turn-on/off time of switching devices, and on-voltage components of switching devices and diodes varies with operating point. In the second phase, the relationship between DTCT and δ-axis dead-time compensation voltage (DTCV) in the current reference frame that is synchronized with current vector has been analyzed and the analytical equation of DTCT has been derived. DTCT is identified on-line with using estimated δ-axis disturbance voltage in current control loop of vector control drive system with the assumption that δ-axis disturbance voltage to be compensated corresponds to δ-axis DTCV. The identified DTCT is utilized for adjusting the amplitude of phase DTCV. In order to confirm validity of the proposed dead-time compensation strategy, simulation and experimental results have been presented. Simulation results have demonstrated that commanded voltage with the proposed dead-time compensation strategy agrees with ideal phase voltage. Experimental results have indicated that active power calculated with using commanded voltage agrees with active power measured with digital power meter within 5% mean absolute percentage error. Compared with conventional adaptive dead-time compensation strategy, the proposed method has the advantage that it has little effect of estimation delay and has expandability for other motor drives, such as the induction motor drive. As in other adaptive methods, the proposed method requires intensive computation. An implementation of system by field programmable gate array (FPGA) can relieve the problem.

References

[1] J.-S. Lee, T. Takeshita, and N. Matsui, "Stator-flux-oriented sensorless induction motor drive for optimum low-speed performance," *IEEE Trans. Ind. Applicat.*, vol. 33, no. 5, pp. 1170–1176, Sep./Oct. 1997.

[2] J. Holtz and J. Quan, "Sensorless vector control of induction motors at very low speed using a nonlinear inverter model and parameter identification," *IEEE Trans. Ind. Applicat.*, vol. 38, no. 4, pp. 1087–1095, Jul./Aug. 2002.

[3] L. Zhong, M. F. Rahman, W. Y. Hu, and K. W. Lim, "Analysis of direct torque control in permanent magnet synchronous motor drives," *IEEE Trans. Power Electron.*, vol. 12, no. 3, pp. 528–536, May 1997.

[4] T. Sukegawa, K. Kamiyama, K. Mizuno, T. Matsui, and T. Okuyama, "Fully digital vector-controlled PWM VSI fed ac drives with an inverter dead-time compensation strategy," *IEEE Trans. Ind. Applicat.*, vol. 27, no. 3, pp. 552–559, May/Jun. 1991.

[5] S.-G. Jeong and M.-H. Park, "The analysis and compensation of dead-time effects in PWM inverters," *IEEE Trans. Ind. Electron.*, vol. 38, no. 2, pp. 108–114, Apr. 1991.

[6] R. B. Sepe and J. H. Lang, "Inverter nonlinearities and discrete-time vector control," *IEEE Trans. Ind. Applicat.*, vol. 30, no. 1, pp. 62–70, Jan./Feb. 1994.

[7] R. J. Kerkman, D. Leggate, D. W. Schlegel, and C. Winterhalter, "Effects of parasitics on the control of voltage source inverter," *IEEE Trans. Power Electron.*, vol. 18, no. 1, pp. 140–150, Jan. 2003.

[8] J.-W. Choi and S.-K. Sul, "Inverter output voltage synthesis using novel dead time compensation," *IEEE Trans. Power Electron.*, vol. 11, no. 2, pp. 221–227, Mar. 1996.

[9] A. R. Munoz and T. A. Lipo, "On-line dead-time compensation technique for open-loop PWM-VSI drive," *IEEE Trans. Power Electron.*, vol. 14, no. 4, pp. 683–689, Jul. 1999.

[10] H. Zhao, Q. M. J. Wu, and A. Kawamura, "An accurate approach of nonlinearity compensation for VSI inverter output voltage," *IEEE Trans. Power Electron.*, vol. 19, no. 4, pp. 1029–1035, Jul. 2004.

[11] H.-S. Kim, H.-T. Moon, and M.-J. Youn, "On-line dead-time compensation method using disturbance observer," *IEEE Trans. Power. Electron.*, vol. 18, no. 6, pp. 1136–1345, Nov. 2003.

Naomitsu Urasaki (M'98) was born in Okinawa, Japan, in 1973. He received the B.S., M.S., and Ph.D. degrees in electrical engineering from the University of the Ryukyus, Okinawa, Japan, in 1996, 1998, and 2004, respectively.

Since 1998, he has been with Department of Electrical and Electronics Engineering, Faculty of Engineering, University of the Ryukyus, where he is currently a Research Associate. His research interests are in the areas of motor drives.

Dr. Urasaki is a member of the Institute of Electrical Engineers of Japan.

Tomonobu Senjyu (M'02) was born in Saga, Japan in 1963. He received the B.S. and M.S. degrees in electrical engineering from University of the Ryukyus, Okinawa, Japan, in 1986 and 1988, respectively, and the Ph.D. degree in electrical engineering from Nagoya University, Nagoya, Japan, in 1994.

Since 1988, he has been with the Department of Electrical and Electronic Engineering, Faculty of Engineering, University of the Ryukyus, where he is currently a Professor. His research interests are in the areas of stability of ac machines, advanced control of electrical machines, and power electronics.

Dr. Senjyu is a member of the Institute of Electrical Engineers of Japan.

Katsumi Uezato was born in Okinawa, Japan, in 1940. He received the B.S. degree in electrical engineering from the University of the Ryukyus, Okinawa, in 1963, the M.S. degree in electrical engineering from Kagoshima University, Kagoshima, Japan, in 1972, and the Ph.D. degree in electrical engineering form Nagoya University, Nagoya, Japan, in 1983.

Since 1972, he has been with the Department of Electrical and Electronic Engineering, Faculty of Engineering, University of the Ryukyus, where he is currently a Professor. He is engaged in research on stability and control of synchronous machines.

Dr. Uezato is a member of the Institute of Electrical Engineers of Japan.

Toshihisa Funabashi (M'90–SM'96) was born in Aichi, Japan, in 1951. He received the B.S. degree in electrical engineering from Nagoya University, Aichi, Japan in 1975 and the Ph.D. degree in electrical engineering from Doshisha University, Kyoto, Japan, in 2000.

In 1975, he joined Meidensha Corporation, Tokyo, Japan, where he was engaged in research on power system analysis and is currently Senior Engineer of the Power System Engineering Division.

Dr. Funabashi is a Chartered Engineer in the U.K. and a member of the IEE and the IEE of Japan.